Ocean Engineering 178 (2019) 331–344

Contents lists available at ScienceDirect

Ocean Engineering

journal homepage: www.elsevier.com/locate/oceaneng

Experimental analysis of the squat of ships advancing through the New Suez Canal

Khaled Elsherbiny[a,b,*], Tahsin Tezdogan[a], Mohamed Kotb[b], Atilla Incecik[a], Sandy Day[a]

[a] Department of Naval Architecture, Ocean and Marine Engineering, Henry Dyer Building, University of Strathclyde, 100 Montrose Street, Glasgow, G4 0LZ, UK
[b] Department of Marine Engineering, College of Engineering and Technology, Arab Academy for Science, Technology and Maritime Transport, Abo Kir, Alexandria, P.O. Box 1029, Egypt

ARTICLE INFO

Keywords:
Squat prediction
Experiments
New suez Canal
Model-scale KCS

ABSTRACT

As a ship travels forward, squat of the ship may occur due to an increase in sinkage and trim. Squat is a crucial factor that restricts ship navigation in shallow water. A new division of the Suez Canal, the New Suez Canal, recently opened for international navigation. It is important to obtain accurate prediction data for ship squat to minimise the risk of grounding in this canal.

To provide guidance for shipping in canals a series of experiments was conducted on a model scale of the Kriso Container Ship (KCS). The squat of the KCS was examined by measuring its sinkage and trim. A wide range of water depth to ship draft ratios at various ship speeds was investigated. Additionally, the blockage effect was studied by varying the canal width, and deep water tests were performed. The results indicated that for Froude's number based on depth (Fn_h) below 0.4, measured squat value do not change with either Fn_h or depth to draft ratio (H/T). The squat increases with H/T values for Froude numbers higher than 0.4. Moreover, a canal with reduced width had a negligible effect on squat, suggesting that the next segment of the Suez Canal can be built to a narrower width.

1. Introduction

1.1. New Suez Canal

The Suez Canal is located in Egypt, west of the Sinai Peninsula. It connects Port Said on the Mediterranean Sea with the port of Suez on the Red Sea, and provides an essentially direct route for the transport of goods between Europe and Asia. Fig. 1 shows the Suez Canal's location, while Fig. 2 shows its cross section. Table 1 includes Suez Canal main dimensions in addition to the maximum ship speed and draft permitted. The canal supports approximately 8% of the world's shipping traffic with almost fifty vessels travelling through the canal each day (from Suez Canal Authority website, March 2018).

A new shipping lane (termed the New Suez Canal) was added to the Suez Canal and inaugurated on 5 August 2014. In addition, other parts of the Suez Canal were made deeper and wider (from Suez Canal Authority website, March 2018).

The idea of the project was to construct a new canal parallel to the old one. The new canal is 72 km long. The New Suez Canal is expected to expand trade along the fastest shipping route between Europe and Asia. The new canal allows ships to sail in both directions at the same time. This decreases the transit time from 18 h to 11 h for the southbound convoy. It also shortens the waiting time for vessels down to a maximum of 3 h, rather than the previous 8–11 h. This will cut down on trip costs and make the Suez Canal more attractive for ship owners. The New Suez Canal is expected to virtually double the capacity of the Suez Canal from 49 to 97 ships a day.

1.2. Squat phenomenon

The phenomenon of squat is caused in shallow water when the clearance between a ship's keel and the seabed decreases. A combination of the sinkage and trim angle variation in shallow water is called ship squat (Barrass, C.B., and Derret, D.R., 2012). In the first place this phenomenon occurs due to appreciable change in potential flow around the hull. If the ship is considered as being at rest in a flowing stream of restricted depth, but unrestricted width, the water passing below it must speed up more than in deep water, with a consequent great reduction in pressure. As per Bernoulli's theorem (Larsson, L., et al., 2010), if the flow velocity (Vs) increases in a flowing liquid, the

* Corresponding author. Department of Naval Architecture, Ocean and Marine Engineering, Henry Dyer Building, University of Strathclyde, 100 Montrose Street, Glasgow, G4 0LZ, UK.
E-mail addresses: khaled.elsherbiny@strath.ac.uk, khaled.elsherbiny@aast.edu (K. Elsherbiny).

https://doi.org/10.1016/j.oceaneng.2019.02.078
Received 3 November 2018; Received in revised form 27 February 2019; Accepted 28 February 2019

Fig. 1. Suez Canal location (from Suez Canal Authority website, March 2018).

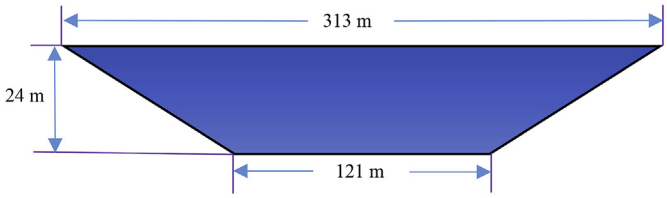

Fig. 2. Suez Canal cross sectional area.

Table 1
Suez Canal Characteristics (from Suez Canal Authority website, March 2018).

Parameter	Unit	Value
Overall length	km	193.30
Double path length	km	113.3
The width range along the canal at 11 m depth	m	205–225
Water depth	m	24
Max. Draft of ship	m	20.12
The cross sectional area range along the canal	m^2	4800–5200
Max. Loaded ship	DWT	240,000
Vessel speed	knot	7
Maximum boat beam	m	77.5
Distance between two ships	km	2

pressure in the region decreases. As the pressure (P) at the bottom of the ship decreases, the ship needs to react in some manner to compensate for this. Ships float because the net forces acting on the ship are zero because the force of gravity equals the force of buoyancy. This drop in pressure is compensated by the sinkage of the vessel as the direction of this force (low pressure) is downwards (see Fig. 3). If, in addition, the water is restricted laterally, as in a river or canal, these effects are exaggerated. A reduction in ship speed may be observed when a ship enters a shallow water condition. This reduction may be as much as 30% if a ship is travelling in open water. If the ship is advancing through a confined channel such as river or a canal, this reduction may rise to 60%. It should be noted that this reduction in speed is not only due to the increase in resistance, but also due to the change in the manoeuvring features of the vessel due to it entering a shallow water area as pointed out in (Tezdogan, T., et al., 2015).

The ship squat phenomenon has been known for some time. Accurate determination of ship squat is required when navigating vessels through shallow water regions, such as rivers, channels and harbours. More than 117 ships have been reported as grounded over the past 40 years, mostly due to squat as pointed out in (Barrass, C.B., and Derret, D.R., 2012). In 1992, QE2 was grounded due to flooding of the tanks in the bow (Kazerooni, M.F. and Seif, M.S., 2014). This was due to extreme squat and draft in the ship forepeak, with the financial loss evaluated at £20 million. These examples demonstrate that accurate prediction of ship squat is essential. More recently, some grounding of ships in the Suez Canal have been recorded and published in World Maritime News (from World Maritime News website, March 2016). A 163,038 DWT oil tanker ran aground 159 km into the Suez Canal in May 2016. Similarly, a 182,307 DWT bulker Eibhlin ran aground during its transit of the Suez Canal with the Southbound convoy. Finally, in April 2016, a 153,514 DWT containership MSC Fabiola had a similar fate. For this reason it is very important that the Suez Canal authorities have accurate prediction data for ship squat to minimise the risk of grounding for ships.

There are various methods available to predict ship squat and resistance in shallow water. These methods include empirical formulae, analytical, numerical and experimental methods. Empirical formulae can quickly estimate the squat according to the ship dimensions, ship coefficients, ship speed and water depth. These formulae are obtained from a series of model tests, but these formulae still have certain conditions and constraints to be satisfied before they can be applied. The analytical method mainly uses assumptions based on simple potential theory such as slender body theory. The numerical method or Computational Fluid Dynamics (CFD) methods have been more recently developed and can be easily used for predicting a ship's squat. The experimental methods are more accurate to simulate and predict squat phenomena. In this paper, a series of experimental tests are carried out on a container ship model to study ship squat and resistance characteristics while navigating the New Suez Canal.

Factors governing ship squat include ship speed, water depth, block coefficient and blockage ratio (K) given by Equation (1) (see Fig. 4);

$$K = \frac{b^*T}{B^*H} \tag{1}$$

Where b is the ship's breadth, T is the ship's draft, B is the canal's breadth and H is the depth of the water.

The New Suez Canal was opened on August 6th, 2015 for international navigation. It will therefore be very useful to investigate the squat phenomena in the new part of the canal to avoid any future problems that may arise due to the variation in the seabed depth and/or a vessel's speed. To the best of our knowledge, no studies on this phenomenon are currently available in the open literature.

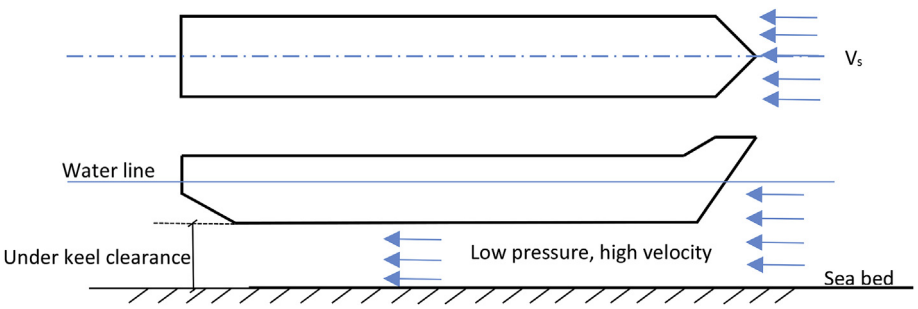

Fig. 3. Squat effect on ships in shallow water.

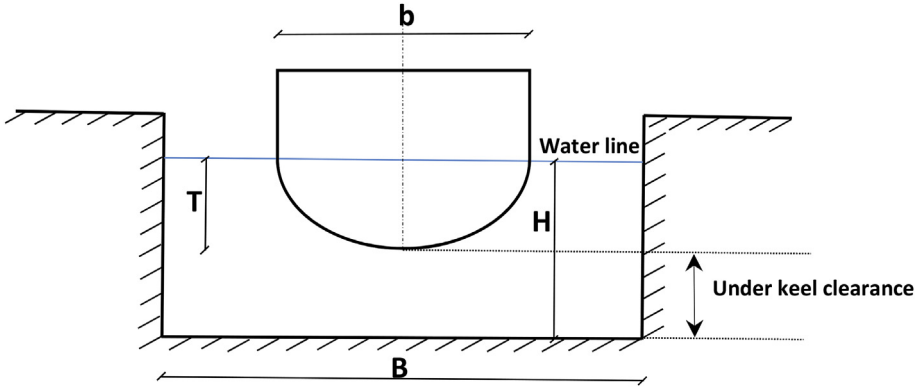

Fig. 4. A ship in a canal.

2. Background

A second effect of ship squat is that changes in a ship's wave pattern occur when passing from deep water to shallow water. These changes have been studied by Havelock, TH (1908) for a point pressure impulse travelling over a free water surface. Havelock examined the wave patterns in shallow water by taking into account the speed of the vessel, and the depth of water, which led to the introduction of the depth Froude number (Fn_h), Equation (2).

$$Fn_h = \frac{u}{\sqrt{gH}} \tag{2}$$

Where u is the speed of the vessel (m/s), g is the acceleration due to gravity (m/s^2) and H is the water depth. The wave pattern is enclosed between straight lines having angles equal to 19° 28 min (as seen in Fig. 5a) when the Froude number is less than 0.4 (subcritical speeds). The angle of the wave pattern increases and approaches 90° (as seen in Fig. 5b) when the Froude number is equal to 1 (critical speeds). The angle of the wave pattern begins to decrease again (as seen in Fig. 5c) when the Froude number is more than 1 (supercritical speeds).

Many researchers have investigated ship squat in restricted water. Constantine, T. (1961) studied the different behaviour of ship squat for various ship speeds (subcritical, critical and supercritical) and the ratio of midship section to the cross section of the fairway. Tuck, E.O. (1966) calculated the flow around a slender hull in shallow water and devised formulae to predict the wave resistance, sinkage and trim at subcritical and supercritical speeds. Millward, A. (1996) presented an overview on the general problem of a ship in shallow water and developed an expression for maximum bow squat in laterally unrestricted water based on model tests with various ship speeds. Gourlay (2008c) used a theoretical method based on the linear superposition of slender-body shallow-water flow solutions to predict the sinkage and trim of two moving ships as they pass each other, either from opposite directions, or one ship overtaking the other. Delefortrie, G., et al. (2010) investigated the squat when a ship is sailing in a muddy area. Lataire, E., et al. (2012) predicted the squat for a wide range of water depths and widths of a canal with rectangular cross section using an experimental method for a model scale KVLCC2. JI, S.C., et al. (2012) predicted the relationship between these geometrical and kinematical parameters and the amplitude of ship-generated waves, and the water plane drawdown, by simulating wave patterns induced by moving convoys composed of one or two barges in restricted waterways. This was done by numerical simulations which were conducted by solving the 3-D Navier-Stokes equations along with the standard k-ε turbulence model. Kazerooni, M.F. and Seif, M.S., (2013) measured and analysed the squat phenomenon by using model tests for a tanker ship model and Dhow model performed in a towing tank. The squat data was investigated and have been plotted versus under keel clearance for various Froude numbers. However, it is observed that high scale factors were utilised; 176 for tanker model and 84.5 for Dhow model. Therefore, further study using reasonably scaled models must be conducted to evaluate these findings. Sergent, P., et al. (2014) proposed a new mathematical expression from a 2D analytical model to evaluate the unstable equilibrium position of a ship during heave motions as a function of canal and ship parameters. Tezdogan, T., et al. (2015) predicted the squat and resistance of a model scale container ship advancing in a canal using a numerical method based on nonlinear unsteady RANS simulations. Gourlay (2008b) published a review paper of predicting ship squat in shallow open water at subcritical speeds using linear slender-body methods. Additionally, Gourlay (2008a) developed a numerical method using a linear slender-body theory to predict the sinkage and trim of a fast displacement catamaran running in shallow open water for various ship speeds (subcritical, critical and supercritical). Gourlay assumed that the developed theory can be used to produce guidelines to predict the maximum squat of any fast displacement catamaran model. Alderf, N., et al. (2011) developed a new method for the numerical modelling of dynamic squat by using a finite element method. Alderf also illustrated the effect of sea floor topology on a ship sailing at critical speed. This model

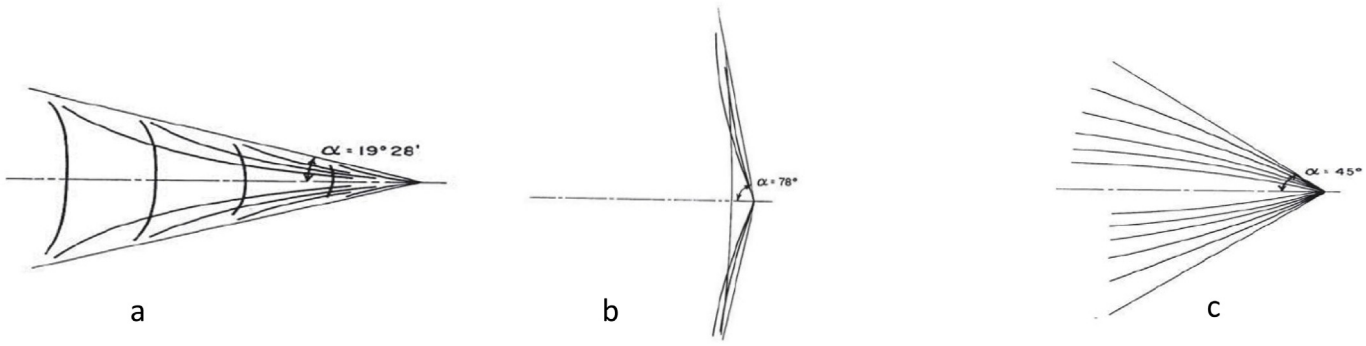

Fig. 5. Wave pattern a) $Fn_h < 0.4$, b) $Fn_h = 1$, c) $Fn_h > 1$ (Larsson, L., et al., 2010).

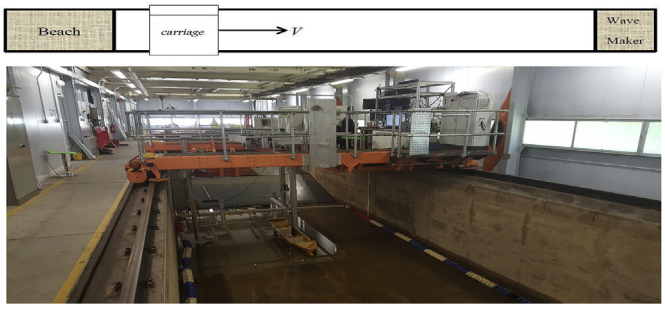

Fig. 6. The Kelvin Hydrodynamics lab.

can give results for the dynamic responses of a ship in highly restricted canals on any seafloor shape.

3. Experimental setup

3.1. Towing tank

This work's experiments were conducted at the Kelvin Hydrodynamics Lab at the University of Strathclyde. The towing tank is 76 m long and 4.6 m wide (see Fig. 6). The water depth at the tank was set at 0.32 m for shallow water tests and 2.3 m for deep water tests.

The tank was prepared for four test conditions:

Case I: The tank cross section is rectangular (4.6 m wide and 0.32 m water depth). This is to simulate water depth effects only on ship sailing characteristics. Channel bank effects are excluded. (Refer to Fig. 7a).

Case II: Channel banks are introduced through side planks. This configuration is intended to test the effects of both water depth and width (blockage effects) (refer to Table 2). This case also aims to simulate the cross sectional area of the New Suez Canal. it was prepared at a scale of 1:75 with respect to its real dimensions. (Refer to Fig. 7b and c).

Case III: As per Case II but with reduced water surface width and bottom width. This case was designed for studying higher blockage ratios. (Refer to Fig. 7d and Table 2).

Case IV: The tank is filled with water to 2.3 m deep with 4.6 m water surface width. These configurations are intended to test deep water motion characteristics. (Refer to Fig. 7e).

Where $\bar{B}$ is mean tank width.

3.2. Model and experimental test setup

A KCS model was used to study squat characteristics test (see Fig. 8a). Full scale and model scale particulars are given in Table 3. The model tests are carried out at a range of ship speeds (see Table 4) and ship drafts.

Two LVDTs (Linear Variable Differential Transformer) were employed to measure trim and sinkage. The sinkage LVDT1 was attached at the mid ship point to measure the heave motion in dynamic mode and the trim LVDT2 was attached at the model forepeak, using the configuration as illustrated in Fig. 8b. The trim angle was then calculated according to Equation (3).

$$Trim = tan^{-1}\left(\frac{L_2 - L_1}{d}\right) \tag{3}$$

where L_1 and L_2 are the $LVDT_1$ and $LVDT_2$ vertical displacement, respectively.

A load cell was used to measure the water resistance force. This load cell was attached at the mid ship point. The model was restricted to move only in the vertical plane (heave and pitch motion) while being restricted in all other directions. One of the main features of the model test in the towing tank is the possibility of extrapolating the results to the full scale, because in this test the Suez Canal cross section and KCS model were constructed with scale factor 75. It should be noted that the Reynolds number (Re) for the full scale KCS ship at 7 knots calculated to be 668,096,334.3 and the Reynolds number for the model scale is 1,073,129.8. The formulation of Reynolds number given in equation (4).

$$Re = \frac{u * L}{\upsilon} \tag{4}$$

where L is the model ship length water line and υ is the water kinematic viscosity which is equal to 1.2532×10^{-6} for seawater and 1.2012×10^{-6} for fresh water at 13 C° which was the temperature of water during the test (ITTC- Fresh Water and Seawater Properties (2011).

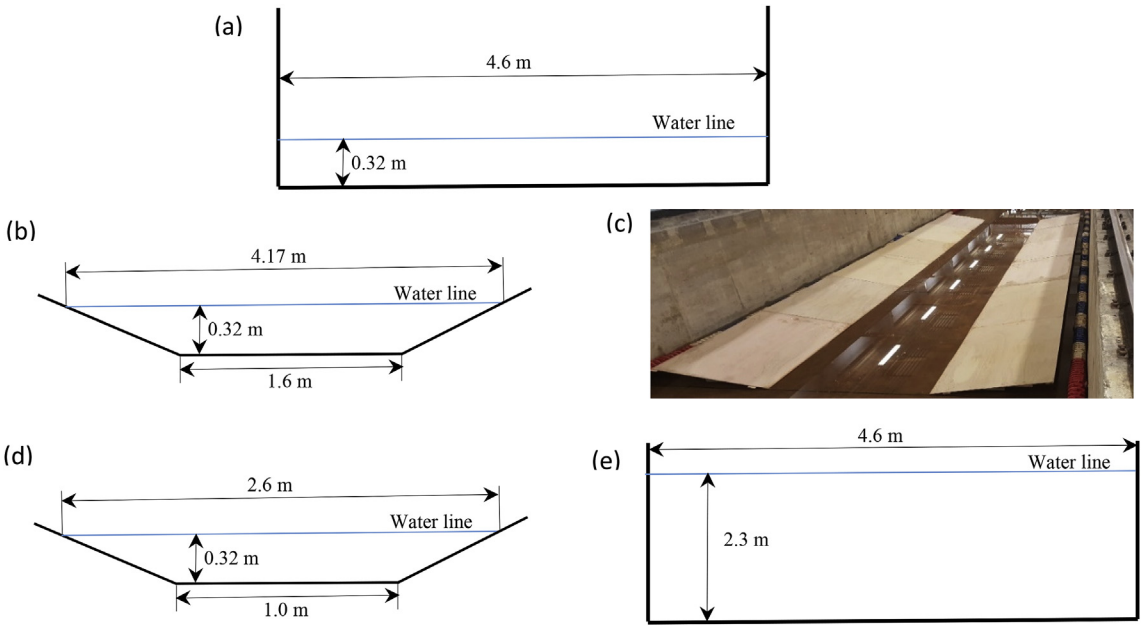

Fig. 7. Depictions of the four cases with schematic drawing; a: case I, b & c: case II, d: case III, e: case IV.

Table 2
Blockage effect for all cases at H/T = 0.144.

		Model		Tank		Cross sectional area		Blockage ratio (K)
H/T	Case	b (m)	T (m)	$\bar{B}$ (m)	H (m)	A_m (m^2)	A_{tank} (m^2)	$(b * T)/(\bar{B} * H)$
1.78	I	0.429	0.144	4.6	0.32	0.062	1.472	0.042
1.78	II	0.429	0.144	2.88	0.32	0.062	0.8448	0.067
1.78	III	0.429	0.144	1.8	0.32	0.062	0.576	0.10,725
15.97	IV	0.429	0.144	4.6	2.3	0.062	10.58	0.0058

Fig. 8. *B schematic* drawing *for trim and sinkage measurements using LVDTs.*

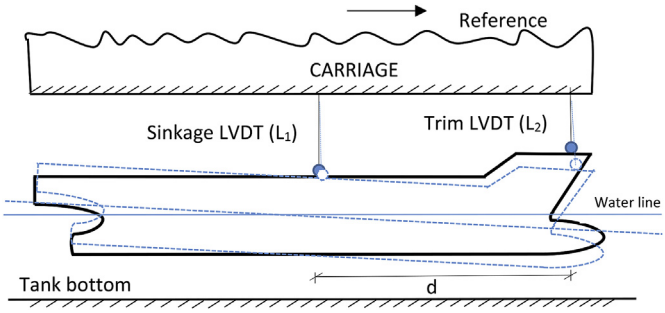

Fig. 8. (*continued*)

Table 3
KCS main particulars (from SIMMAN, 2008).

Parameters	Full scale	Model scale with scale factor 1:75
Length between perpendiculars (m)	230	3.067
Length at water line (m)	232.5	3.1
Breadth at water line (m)	32.2	0.429
Depth (m)	19	0.25
Draft (m)	10.8	0.144
Displacement (m^3)	52,030	0.123
Wetted surface area w/o rudder (m^2)	9530	1.694
Block Coefficient	0.651	0.651
Midship section area Coefficient	0.985	0.985
Longitudinal centre of buoyancy (%), fwd+	−1.48	−1.48

4. Calibration of equipment

Before performing any runs, it is of key importance to check the precision and calibration of the measuring devices used for the tests. These are composed mostly of strain transducers and motion sensors.

4.1. LVDT calibration

Firstly, calibration of the vertical motion sensor used to measure the amplitudes was performed. This was done with a standard distance rule that the arm of the sensor would measure in a stepwise manner. The measuring arm has to only measure the difference between distances to calibrate itself. The standard rule is made extremely precisely and, provided the motion arm is zeroed prior to each test, it can measure distance very precisely. The LVDT for measuring the sinkage and the bow motion were calibrated using a 3D printed block with known distances marked on it. The voltage measured was recorded and the results are shown in Figs. 9 and 10. The systematic error is negligible.

Table 4
Velocity during the test.

Full-scale speed (knots)	Full-scale speed (m/s)	Froude Number for model scale (Fh = U/√(g × H))	Model-scale speed (m/s)
2	1.01	0.067	0.119
3	1.54	0.1	0.178
4	2.06	0.134	0.238
5	2.57	0.167	0.297
6	3.09	0.2	0.356
7	3.6	0.235	0.416
8	4.12	0.268	0.475
9	4.63	0.302	0.535
10	5.14	0.335	0.594
14	7.2	0.469	0.832
17	8.74	0.57	1.010
20	10.29	0.671	1.188
22	11.32	0.738	1.307
23	11.83	0.771	1.366

4.2. Load cell calibration

For the strain transducers calibration, known weights were hung from the device, measuring the voltage induced so that a correlation and a zero value could be found. The weights were increased gradually to produce a proportionality curve for the voltage induced against weight. This allowed the transducer to easily measure force in Newtons. For the load cell, the calibration process consisted of measuring the voltage produced from the change in resistance due to loaded weights from 0.1 to 10 kg 10 kg was chosen as the maximum weight as the predicted maximum resistance was approximately 100 N, therefore the load cell was calibrated to work in the region 0–100 N. The graph from the load cell calibration is shown in Fig. 11 which shows there is

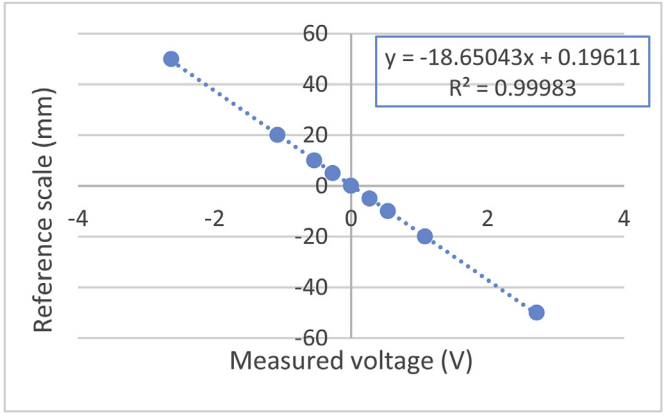

Fig. 9. Calibration result of the LVDT sinkage.

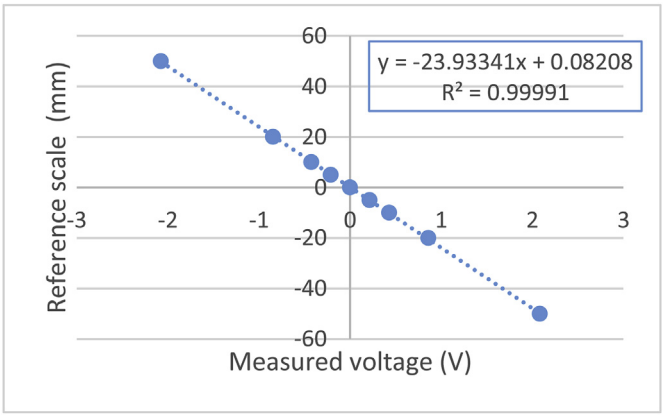

Fig. 10. Calibration results of the LVDT bow.

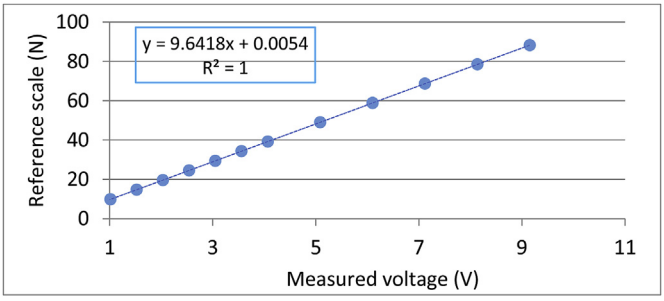

Fig. 11. Load cell calibration.

negligible error in the calibration.

4.3. Uncertainty analysis

It is well known that any experiment designed to determine an effect, validate a theoretical model, or estimate the numerical value of a physical variable will be always affected by errors due to instrumentation and calibration devices. Thus, estimation of experimental uncertainty is needed to assess the confidence in the presented results. The uncertainty is divided into two types A and B, based on the way that the uncertainty is evaluated. Type A is precision and type B is bias as introduced in 'ITTC- Example for Uncertainty Analysis of Resistance Tests in Towing Tank (2014)'.

4.4. Type a standard uncertainty

This is a method of determining standard uncertainty by evaluation of a statistical analysis of a series of repeated observations. This is also termed 'random uncertainty' (ISO GUM, 2008).

Equation (5) shows how to measure uncertainty using the Type A (u_A) method:

$$u_A = \sqrt{\frac{S^2}{i}} \tag{5}$$

where i is the number of repeat observations and S is the standard deviation of the values (see Equation (6)).

$$S = \sqrt{\frac{\sum_{j=1}^{i}(e_j - \bar{e})^2}{i-1}} \tag{6}$$

where e_j is the jth repeated reading and $\bar{e}$ is the mean value of all the repeated readings (see Equation (7)).

$$\bar{e} = \frac{\sum_{j=1}^{i} e_j}{i} \tag{7}$$

To obtain a 95% level of confidence uncertainty, the uncertainty Type A (uA) is multiplied by a coverage factor k as in Equation (8).

$$U_A = ku_A \tag{8}$$

where k = 1.96 for a 95% level of confidence.

4.5. Type B standard uncertainty

This is a method of standard uncertainty obtained by means other than statistical analysis, for example instrument calibration data and linear regression analyses. It is also termed 'systematic uncertainty'.

In the present work, three calibration data sets from the LVDT sinkage, LVDT bow and load cells were used to obtain a standard error of estimate (SEE), then multiplied by 3 to obtain a 95% level of confidence uncertainty as described by 'ITTC- uncertainty analysis instrument calibration 2017'.

A linear relation was then fitted to the calibration data using Equation (9).

$$y = a + bx \tag{9}$$

Where y is the independent variable in physical units, x is the dependent value in volts from a voltmeter, b is the slope and a is the intercept. The result of calibration of the two LVDTs and load cells used in the test are presented in Figs. 9–11.

To obtain a better representation of the statistical character of the data, a residual plot was generated (Equation (10)).

$$Resid = y_i - (a + bx_i) \tag{10}$$

The linear regression prediction limit is simply the standard error of the estimate (SEE) (Equation (11)).

$$SEE = \sqrt{\frac{SS_R}{(N-2)}} \tag{11}$$

where SSR is the sum of the square of the residuals (see Equation (12)) and N is the number of calibration points.

$$SSR = \sum_{i=1}^{N}(y_i - a - bx_i)^2 \tag{12}$$

To calculate Type B with a 95% level of confidence, Equation (13) was used.

$$U_B = SEE * 3 \tag{13}$$

Finally, an evaluation of the standard uncertainty, U, was made using Equation (14).

$$U = \sqrt{U_A^2 + U_B^2} \tag{14}$$

4.6. Combined standard uncertainty

The combined standard uncertainty, U_C (y), is the "standard uncertainty of the result of a measurement when that result is obtained from the values of a number of other quantities, equal to the positive square root of a sum of terms, the terms being the variances or covariances of these other quantities, weighted according to how the measurement result varies with changes in these quantities" (ISO GUM 2008). The combined standard uncertainty is evaluated by the propagation of uncertainty and is given by

$$U_C^2(y) = \sum_{i}^{N}\left(\frac{\partial f}{\partial x_i}\right)^2 u^2(x_i) + 2\sum_{i=1}^{N-1}\sum_{j=i+1}^{N}\left(\frac{\partial f}{\partial x_i}\right)\left(\frac{\partial f}{\partial x_j}\right)u(x_i, x_j) \tag{15}$$

In some situations, the measurement is not measured directly, but is determined from a number N of other quantities X_1, X_2, .., X_N through a function f as:

$$Y = f(X_1, X_2, ..., X_N) \tag{16}$$

Where Y is the experimental result determined from N other quantities of the function. The quantity $\frac{\partial f}{\partial x_i}$ and $\frac{\partial f}{\partial x_j}$ is the partial derivative of f with respect to x_i and x_j and is called the sensitivity coefficient c_i and c_j respectively.

The combined uncertainty equation can be rewritten as:

$$U_C^2(y) = \sum_{i}^{N} c_i^2 u^2(x_i) + 2 \sum_{i=1}^{N-1} \sum_{j=i+1}^{N} c_i c_j u(x_i, x_j) \tag{17}$$

4.7. Trim uncertainty

In the present experiment the trim was measured and combined between two standard uncertainties which came from LVDT sinkage and LVDT bow.

$$U_{trim}^2 = \left(\frac{\partial Trim}{\partial LVDTbow}\right)^2 * U_{Sbow}^2 + \left(\frac{\partial Trim}{\partial LVDTsinkage}\right)^2 * U_{Ssinkage}^2 \tag{18}$$

$$Trim = tan^{-1}\left(\frac{L_2 - L_1}{d}\right) \tag{19}$$

where d is the distance between the two LVDT's (=1666 mm).

4.8. Uncertainty results

In this paper the uncertainty is calculated twice, once at high speed of V = 1.426 m/s and again at a low speed of V = 0.416 m/s.

At high speeds, the uncertainty of sinkage, trim and total resistance has been found to give reasonable values (3.47%, 4.64% and 0.79%) respectively. At low speeds, although the uncertainty of resistance gave a reasonable value (2.20%), the uncertainty for both sinkage and trim were calculated to be more than 90%. This can be justified because at low speeds, the squat is always recorded in the range of 1 or 2 mm. Since Type A uncertainty is the dominant value in the total uncertainty, and is independent of the ship speed, the percentage uncertainty during low speeds will be high when compared to the uncertainty during high speed. This happens due to the LVDT resolution, where the minimum measurable sinkage is quite similar to the ship sinkage during the low speed.

5. Experimental results

5.1. Squat and total resistance coefficients for the KCS in a full tank width with restricted depth (case I)

Fig. 12 shows model sinkage ratio (S/L_{pp}) variations versus depth Froude number for different H/T values. It is clearly noted that, no significant change in the sinkage values occurred over the Froude

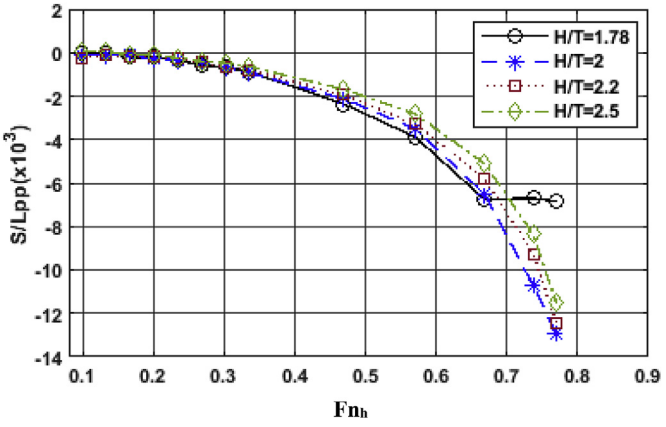

Fig. 12. Sinkage per Lpp vs depth Froude number for different (H/T).

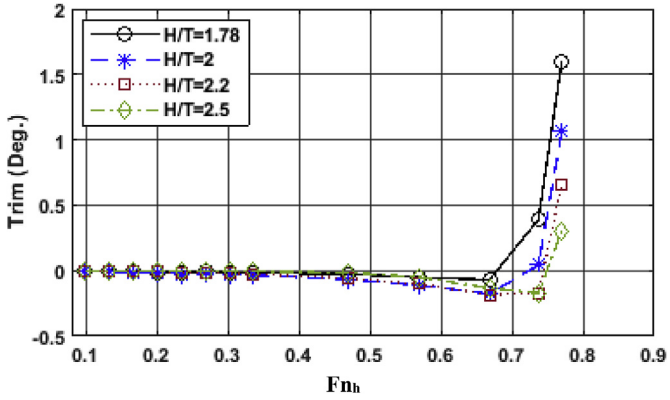

Fig. 13. Trim degree vs Froude Number for different (H/T).

Number range up to 0.33 for all H/T values tested. Past this Fnh range, the sinkage values start to increase with the increase of Fnh and decrease of H/T values.

Fig. 13 presents model trim angle variations against depth Froude number for different H/T values. It can be observed that, similar to the sinkage behaviour described above, trim experiences no significant change up to Froude Number value of 0.4 for all H/T values tested. At Froude Numbers greater than 0.45, the ship trim angle tends to increase by aft. The speed at which trim by bow peak value occurs is subject to the considered H/T value. As the KCS model speed gets higher, the model assumes extreme aft trim angles (Refer to Fig. 14).

It is noteworthy that at high speed Fn > 0.7 the trim by aft assumes extreme values. As a result, at high ship speed the velocity of return flow around the ship section cannot increase further and a pressure waves will be induced in front of the ship model due to accumulates of water in front of ship model (Lataire, E., et al. (2012)) (refer to Fig. 14). Furthermore, as Bernoulli principle, the velocity at ship model stern will decrease and the pressure will increase (Refer to Fig. 14). Albeit, the pressure force acting on the bow will be stronger than on the stern. So, this explains the reason behind getting high aft trim at that low under keel value.

On other hand, the force acting on the ship model stern at sub-critical speeds still not strong enough to create net force at the bow to decrease the sinkage of the model. However, once the blockage effect becomes critical the speed under the keel will became higher and will induce induced high pressure change at stern which leads to high force effect on the ship model stern. Accordingly, the net force acting on the ship model will increase and the sinkage will start to decrease, or remains constant when the blockage ratio exceeds critical value.

To calculate the critical blockage ratio, using Equation (20) (Lataire, E., et al. (2012)).

$$K_{crit} = 1 - \sin\left(3arcsin\left(\frac{Fn_h^{2/3}}{2}\right)\right) \tag{20}$$

At Fn_h = 0.74 the critical blockage ratio K_{crit} is 0.0466 and the actual blockage ratio (K) for the KCS model at H/T = 1.78 is 0.052 which means that the model has exceeded the critical blockage ratio. Observations on Fig. 15 may also help to explain the model behaviour at that speed and blockage ratio.

Fig. 16 displays total resistance coefficient variations versus depth Froude number for different H/T values. Very low values with almost negligible change with respect to both speeds and depth to draft ratios were recorded. The resistance coefficient C_T starts to increase at relatively high rates for Froude Numbers above 0.6 for all H/T values tested. At any Froude Number greater than 0.6, the resistance experienced by the model is proportional to the H/T value. In other words, shallow water effects are more pronounced for smaller values of H/T.

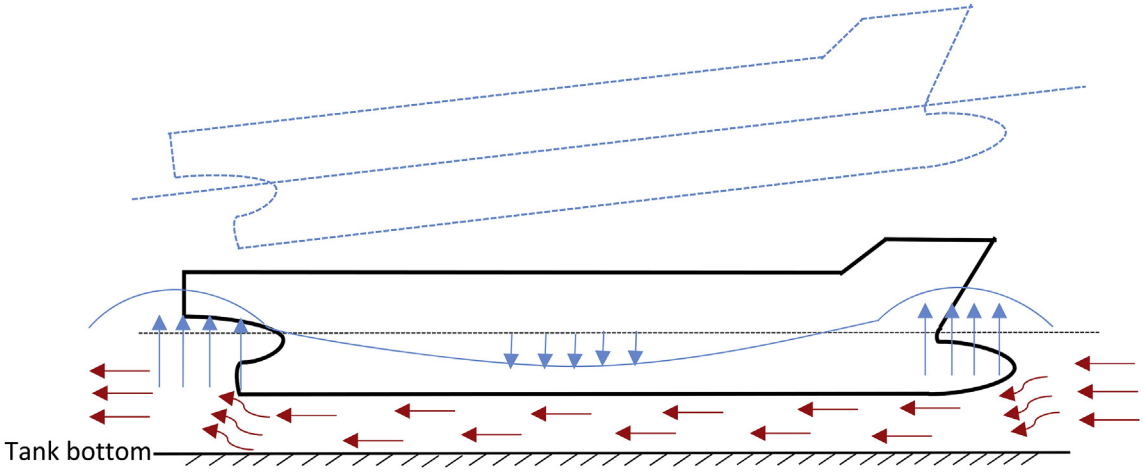

Fig. 14. Schematic drawing for the KCS model at high depth Froude number.

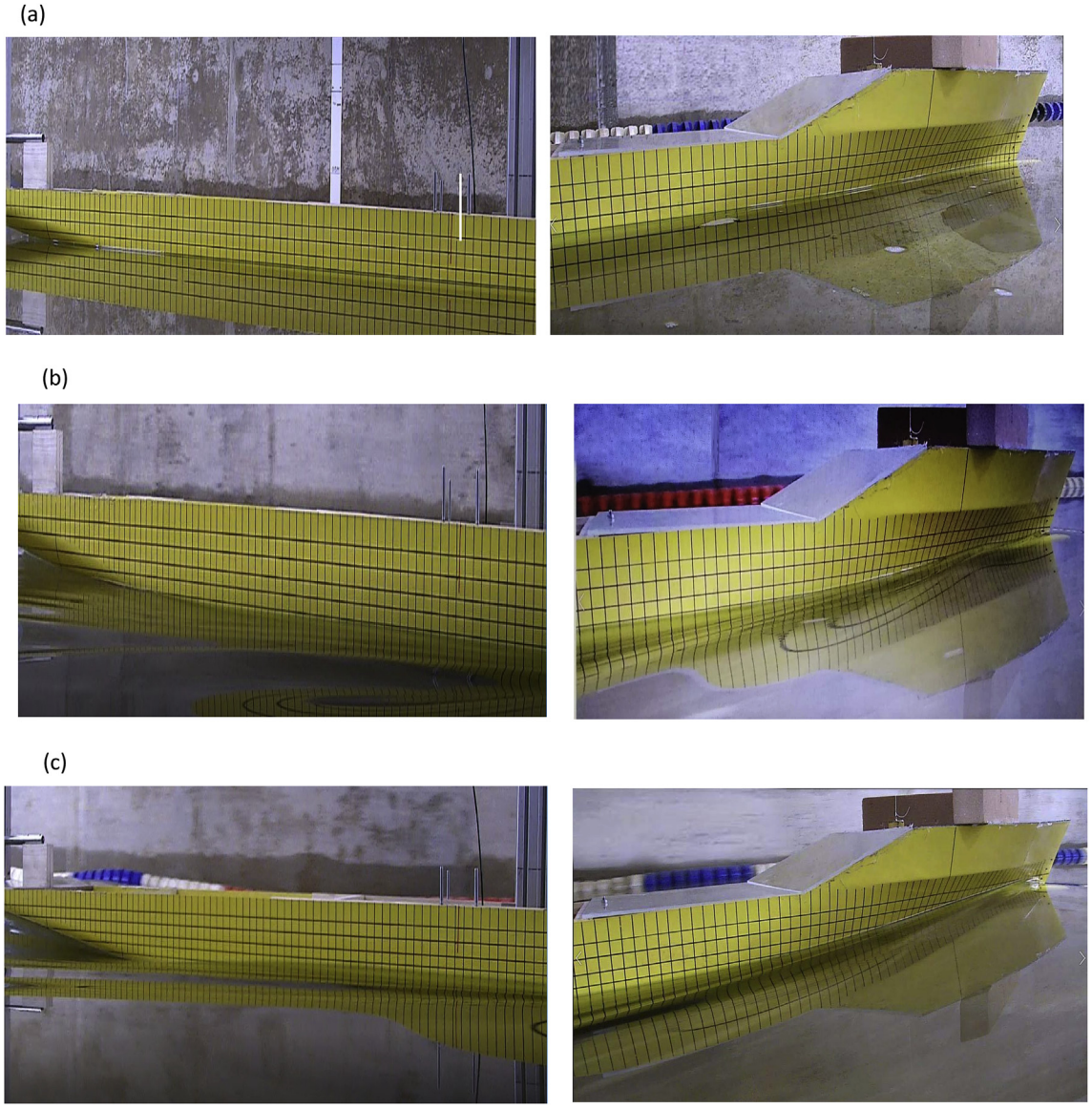

Fig. 15. The KCS model during the experimnts at different depth Froude number a) KCS model with $Fn_h = 0$ and $K_{CRIT} = 1$, b) KCS model with $Fn_h = 0.667$ and $K_{CRIT} = 0.077$ and c) KCS model with $Fn_h = 0.74$ and $K_{Crit} = 0.046$.

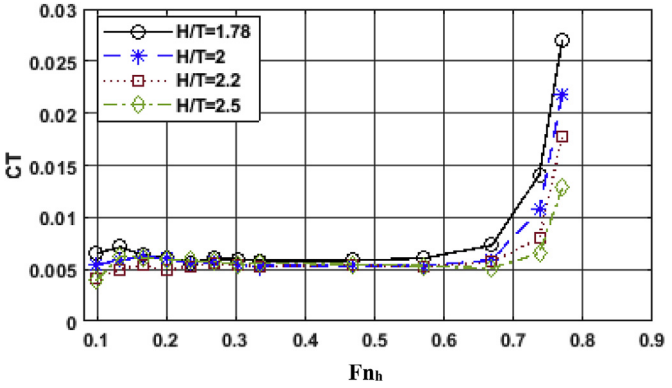

Fig. 16. Total resistance coefficient vs Froude number for different (H/T).

Terziev et al. (2018) presented a numerical study on the DTC container ship in shallow water in order to investigate the sinkage, trim and resistance of ships advancing through restricted shallow water in varying channel cross sections and ship speeds. The authors used Computational Fluid Dynamics (CFD), the Slender-Body theory and various empirical methods to calculate the trim and squat of a containership advancing through different channel geometries. The experimental results presented in the current study are in line with the theoretical findings of Terziev et al. (2018) specifically with respect to a rectangular shaped canal.

Fig. 17 a and b shows the effect of under keel clearance on sinkage and trim where H is water depth and T is ship draft at different model depth Froude Numbers. For low speeds corresponding to deep water depth, depth Froude numbers $Fn_h = 0.235$ and $Fn_h = 0.335$ gave almost no sinkage variations. However, with $Fn_h = 0.771$ the model speed resulted in relatively large sinkage. Trim behaves in a similar way as shown in Fig. 16 (b) for a high speed which corresponds to $Fn_h = 0.768$. The trim degree changes from stern to bow trim as the under keel clearance (H-T)/T decreases (where H is water depth and T is ship draft).

5.2. Comparing the squat and total resistance coefficient between case I and case II at different (H/T)

Fig. 18 a and b show that the more pronounced sinkage and total resistance coefficient are exhibited for Case II where the combined effect of restricted depth and width are manifested for the range of depth Froude numbers tested. Fig. 19 a and b (at H/T = 2.2) exhibit the same trend. This can be explained because as the ship sails through the canal, the blockage effect appears, which is the effect of boundaries on the flow around a ship. This means that the flow speeds increase in the canal to higher than those before the ship entered the canal. According to Conn et al. (1953), the blockage correction, which is the correction of restricted flow caused by boundaries, is unnecessary if Equation (21) is satisfied:

$$B_{model} < \frac{B_{tank}}{10} \rightarrow \frac{B_{tank}}{15} \text{or } T_{model} < \frac{h_{tank}}{10} \rightarrow \frac{h_{tank}}{20} \tag{21}$$

For our case $B_{model} = 0.429m$ and B_{tank} at highest point $= 4.17m$ so $B_{model} > \frac{B_{tank}}{10}$. The same applied for $T_{model} > \frac{h_{tank}}{10}$ so the blockage correction was necessary for our case. To prove the effect of boundaries on the flow in our case we used Conn's method:

$$\left(\frac{V_1}{V}\right)^3 \frac{F_n^2}{2} - \left(1 - \frac{a}{bh} + \frac{F_n^2}{2}\right)\frac{V_1}{V} + 1 = 0 \tag{22}$$

where v = carriage speed, V1 = flow speed after the ship enters the Canal, a = mean cross sectional area of the submerged model, b = tank breadth and h = tank depth.

The flow speed was calculated after entering the Canal at $Fn_h = 0.57$, b at highest point = 4.16 m and h = 0.32 m.

$$\left(\frac{V_1}{1.01}\right)^3 \frac{0.57^2}{2} - \left(1 - \frac{0.0412}{4.16 * 0.32} + \frac{0.57^2}{2}\right)\frac{V_1}{1.01} + 1 = 0 \tag{23}$$

$$0.157672V^3 - 1.12036V + 1 = 0 \tag{24}$$

Solving this equation using Matlab based on the above conditions, a flow velocity $V_1 = 1.06$ m/s results. If we use $\bar{B} = 2.88$ m, which is the mean tank width in the case II, V_1 increases to 1.1 m/s. The underlying reason is the rise in flow velocity after the ship enters the canal. In consequence, the drag force increases since the drag resistance is a function of flow speed (refer to Equation (25) where ρ is water density, C_D is drag coefficient and S is wetted surface area). Drag resistance is one of many factors with an effect on the total resistance of a ship. This explains why the total resistance coefficient increases when the ship enters the Canal.

$$F_d = 0.5\rho C_D S V^2 \tag{25}$$

5.3. Comparing the squat and total resistance coefficient between case II and case III at different (H/T)

The measured squat and total resistance coefficient while moving in realistic canal is plotted versus Froude Number in Figs. 20–22 for three values of H/T ratio for two conditions. The first condition is with the actual cross sectional area of the Suez Canal and the second condition is

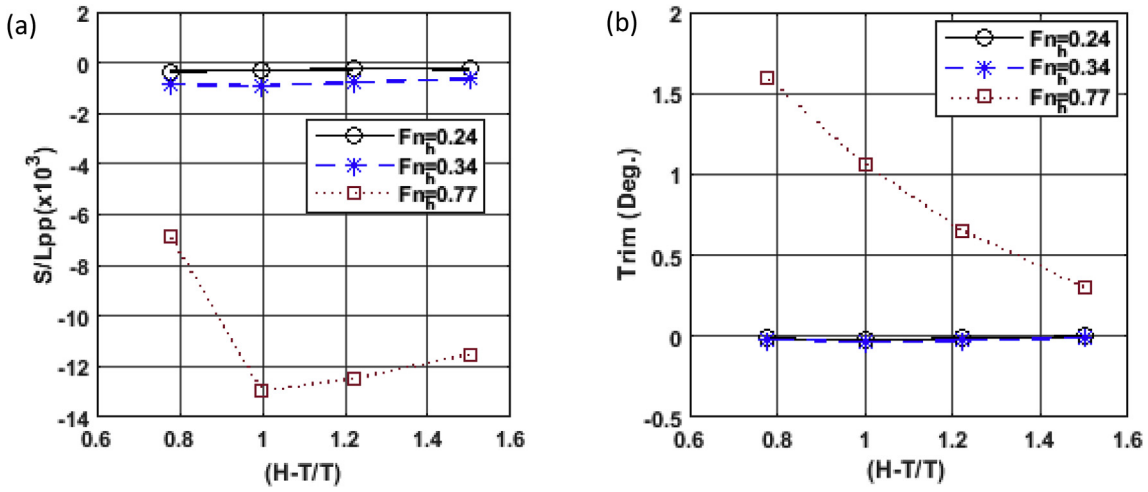

Fig. 17. Effect of under keel clearance on Sinkage (a) and Trim (b) for different Froude numbers.

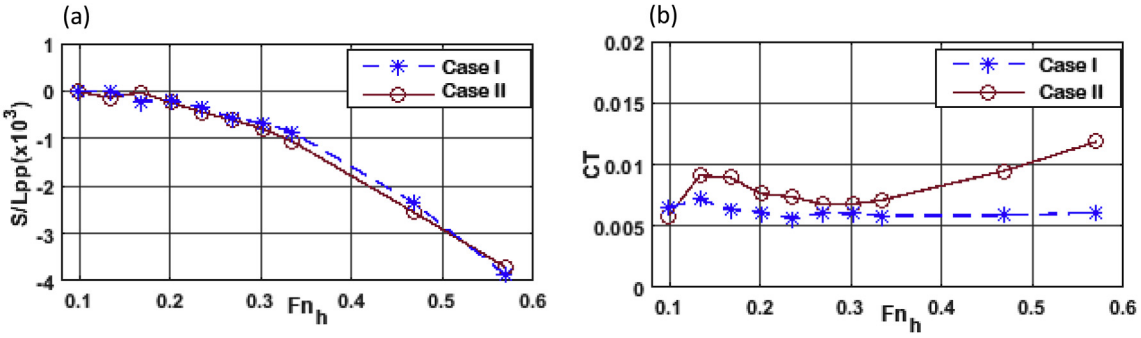

Fig. 18. Effect of Canal on (a) Sinkage and (b) Total resistance coeff. For H/T = 1.78.

after reducing the width of the Canal to 62.5% of its real-life cross sectional area. For the three H/T values it is clearly seen that higher values for the sinkage, trim and total resistance coefficient are recorded for case III due to the effect of higher blockage ratio.

5.4. Form factor

The measured model resistance data was used to determine a form factor value for the KCS. Following the (ITTC – Testing and Extrapolation Methods Resistance, 2002) the wave making resistance coefficient C_W is a function of total resistance coefficient (C_T), friction resistance coefficient (C_F) and form factor (1 + k), as in Equation (26).

$$C_W = C_T - (1 + k)C_F \tag{26}$$

The total resistance coefficient (C_T) and friction coefficient (C_F) were calculated according to the following:

$$C_T = R_T/(0.5 * \rho * S * V^2) \tag{27}$$

where R_T is the model resistance, ρ is the water density, S is the wetted surface and V is model ship speed.

$$C_F = 0.075/(\log Re - 2)^2 \tag{28}$$

A Prohaska test was carried out for two cases of blockage ratio 0.073 and 0.1073 for Case II and Case III respectively for H/T = 2.2. In order to determine the form factor (1 + k) of the KCS hull. It is assumed that at these low speeds the wave making resistance is a function of Fn^4, where Fn is the Froude number based on ship length.

$$F_n = \frac{V}{\sqrt{g * L}} \tag{29}$$

where g is gravitational acceleration.

From Equation (26) the form factor can be found as:

$$(1 + k) = \lim_{F_n \to 0} \frac{C_T}{C_F} \tag{30}$$

In a plot of C_T/C_F versus Fn^4/C_F the value of C_T/C_F at $Fn^4/C_F = 0$ would represent the form factor (1 + k), since the wave making resistance coefficient would equal zero and the total resistance coefficient would represent the viscous resistance coefficient, $C_V = C_F * (1 + k)$. Fig. 23 a and b shows C_T/C_F, where the y-axis intersection is $C_V/C_F = (1 + k)$. (Molland, A. F. 2017).

After fitting a linear trend line through the plot it becomes clear that the resistance tests suggest a form factor (1 + k) = 1.153 for the lower blockage ratio and (1 + k) = 1.603 for the higher blockage ratio.

Fig. 24 shows the side wall effect on the wave making resistance coefficient in shallow water. It can be concluded that the side wall effect on wave making resistance are more significant for Fn_h values greater than 0.35.

It is worth noting that the wave making resistance coefficient curve in the current study shows the same trend as in deep water, as can be found in (Yuan, Z., et al., 2018) which investigated the side wall effects on measurement of wave making resistance for ship model test in towing tank by use of numerical methods based on Rankine type Green function.

As evident from the current study, the effect of side wall on wave making resistance coefficient in shallow water is greater than in deep water at $Fn_h > 0.35$.

Taking into consideration that a KCS ship model is used in the current study, the calculated values of form factor exhibit a similar trend to (Toxopeus, S., 2011) in which computational fluid dynamics (CFD) were employed to calculate the viscous flow for KLVCC2 and showed that form factor varies with condition change from shallow to deep water. It is observed from Fig. 25 that there exists a clearer relation between form factor (1 + k) and water depth to ship model draft ratio (H/T).

5.5. Comparing the squat and drag coefficient between case I and case IV at ship draft 0.144 m

Fig. 26 illustrates model sinkage variations against depth Froude

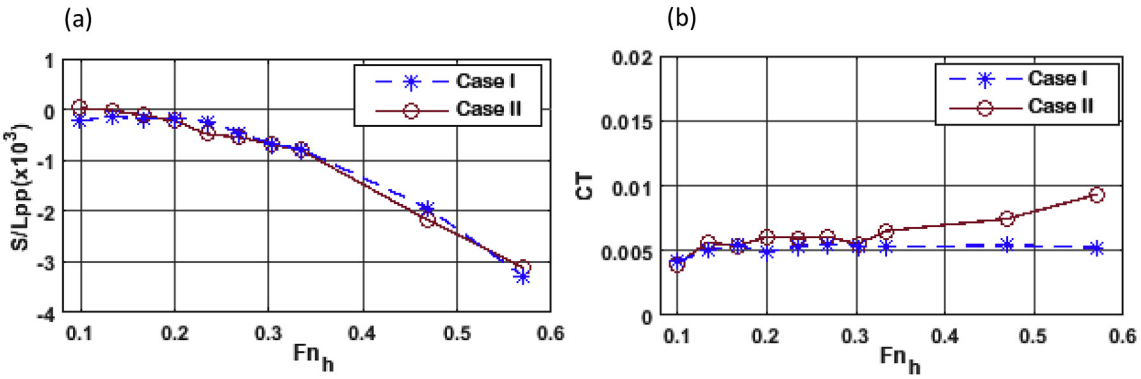

Fig. 19. Effect of Canal on (a) Sinkage and (b) Total resistance coeff. For H/T = 2.2.

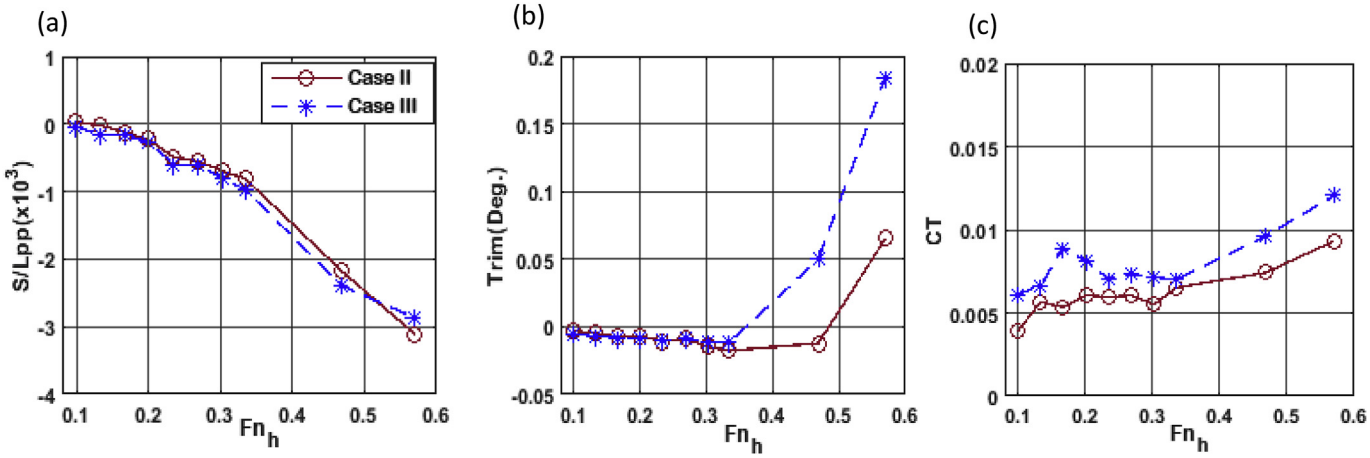

Fig. 20. Side wall effects on (a) Sinkage, (b) Trim and (c) Total Resistance Coeff. For H/T = 2.2.

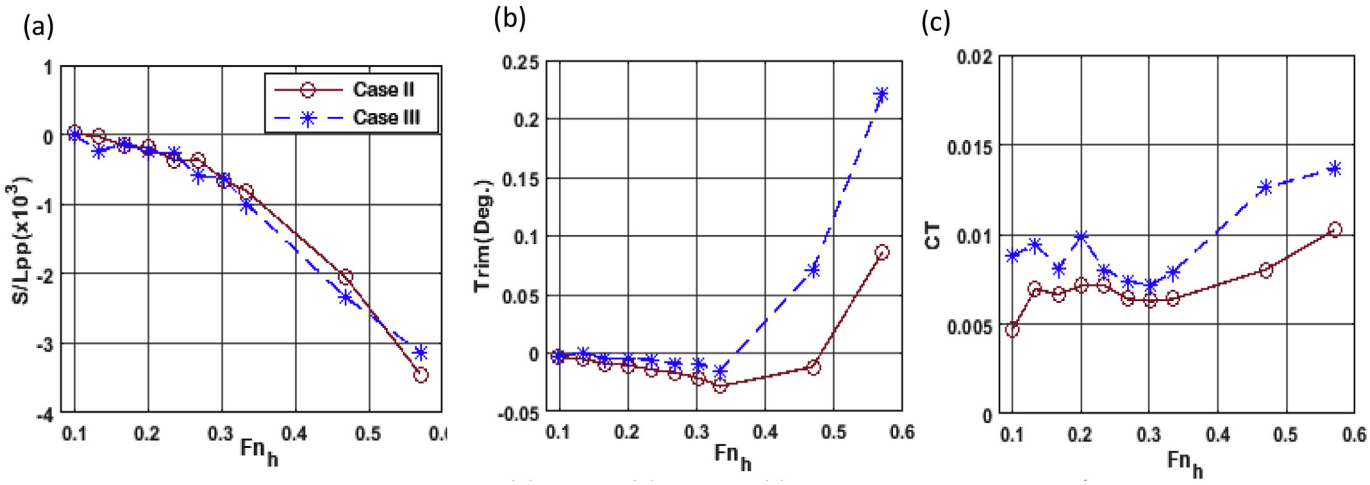

Fig. 21. Side wall effects on (a) Sinkage, (b) Trim and (c) Total Resistance Coeff. For H/T = 2.

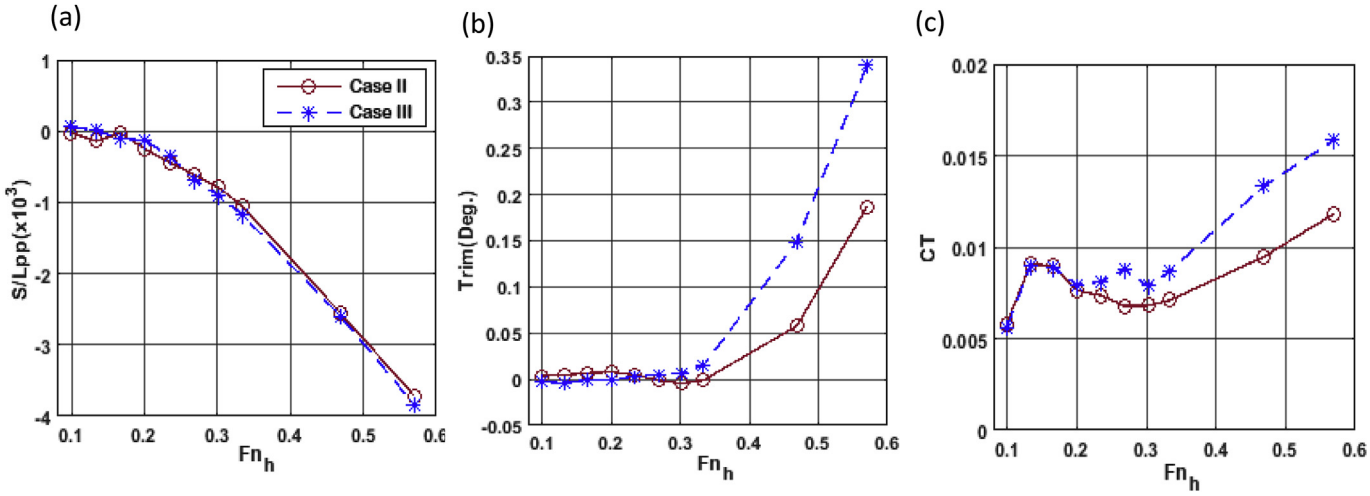

Fig. 22. Side wall effects on (a) Sinkage, (b) Trim and (c) Total Resistance Coeff. For H/T = 1.78.

number for model draft 0.144 m for Case I and Case IV.

Case IV represents mostly deep water behaviour, whereas Case I covers more range of shallow water characteristics manifested in much higher values for Squat.

Fig. 27 illustrates model trim variations against length Froude number for model draft 0.144 m for Case I and Case IV. Similar trend was observed for the trim angles particularly for Case I.

Fig. 28 shows the variations against length Froude number for model draft 0.144 m for Case I and Case IV. Again Case IV results indicated deep water characteristics as no significant variation in total resistance coefficient (C_T) values up to 0.3 Fn_h. On the other hand Case I provide useful data for Total resistance coefficient (C_T) values

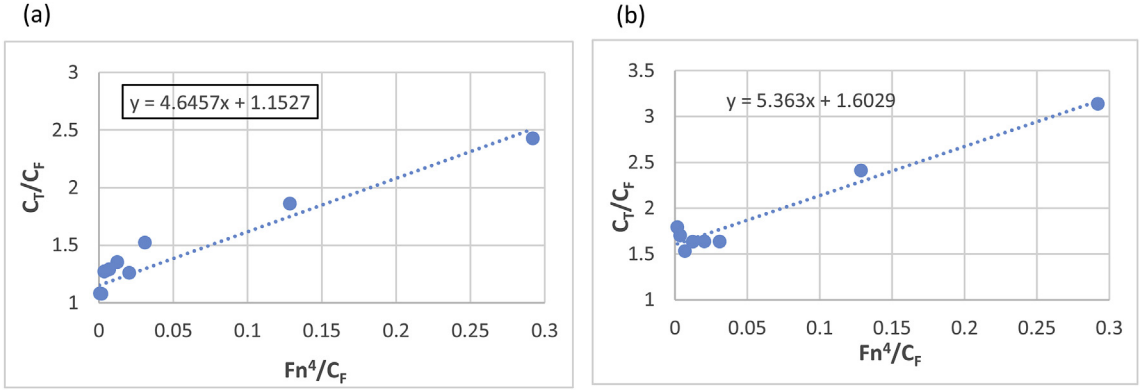

Fig. 23. Form factor calculation (a) blockage ratio = 0.073 (CaseII) and (b) blockage ratio = 0.1073 (CaseIII).

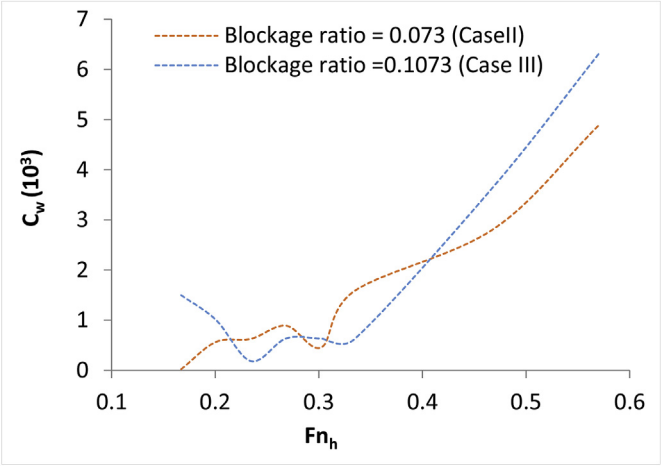

Fig. 24. Side wall effects on wave making resistance coefficient at H/T = 2.2.

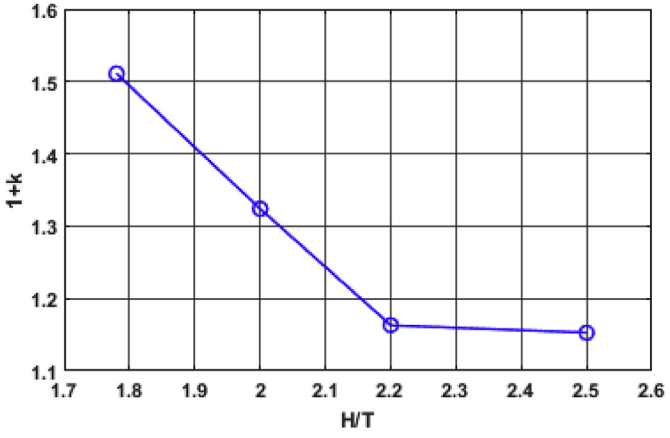

Fig. 25. Effect of change of (H/T) on form factor.

particularly when approaching critical Fn_h values.

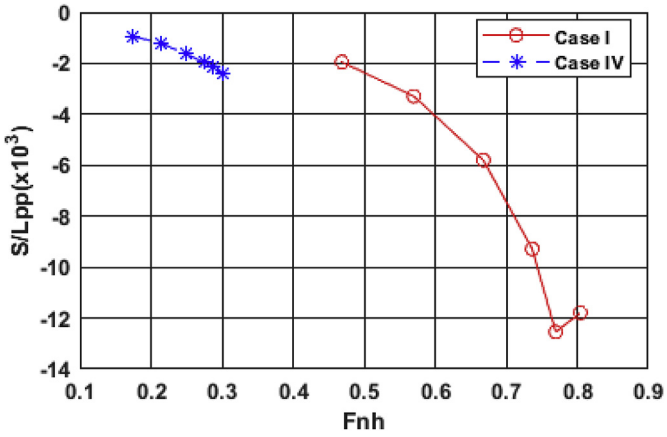

Fig. 26. Sinkage per Lpp vs depth Froude number for draft 0.144 m.

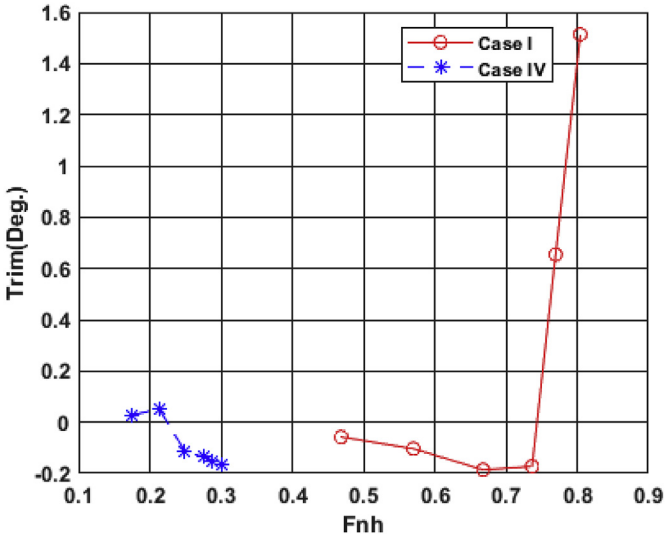

Fig. 27. Trim degree vs depth Froude number for draft 0.144 m.

6. Conclusion and discussion

In conclusion, in this study the squat phenomenon was investigated experimentally in the new Suez Canal under both deep and shallow water operating conditions. The results can be used as a useful database to predict the squat and added resistance of similar ships when navigating the new channel. Several conclusions can be stated.

We found that a smaller keel clearance and higher speed will both significantly increase ship squat. A large trim angle and sinkage was observed when Froude number based on depth exceeded 0.33.

No significant impact on ship sinkage was observed when a ship is inside the canal compared to its former value before the ship entered the canal. Nonetheless, the total resistance force was seen to increase after the ship entered the canal due to blockage effects.

A ship's speed can be increased to up to 9 knots inside the Canal with no adverse effects, thus significantly reducing the time for a ship to pass through the Canal.

After reducing the Canal width to 62.5% of its real-life cross

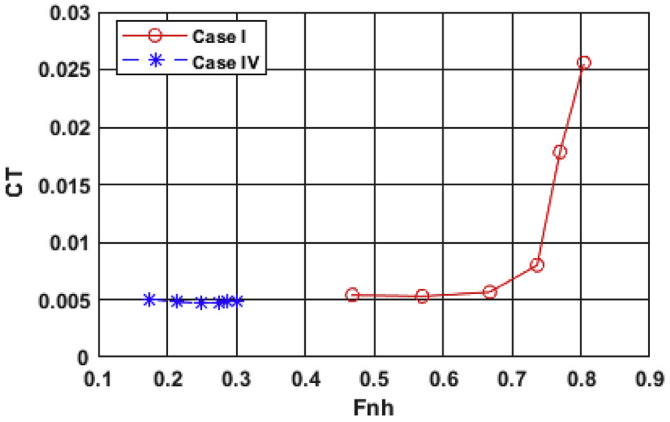

Fig. 28. Total resistance Coefficient vs depth Froude number for draft = 0.144 m

sectional area, no significant effect was observed on ship squat.

Two factors were studied in this study to examine their effects on ship navigating the Suez Canal. There are water depth and cannel width.

Experimental test results confirmed the fact that when the model is moving in deep water ($Fn_h < 0.4$) wave pattern generated by ship motion doesn't change and accordingly almost no effect on sinkage, trim, and resistance.

Two blockage values were also studied to examine canal bank proximity to navigation course effect as for as sinkage, trim and add resistance.

It was found out that higher blockage ratio results in significant squat, trim and added resistance (e.g. 20% increase in wave making resistance for the higher blockage values (0.1073) then the lower are (0.073) at depth Froude number = 0.57). The maximum rate of increase in wave making resistance relative to blockage factor (k) according to (Fig. 24) can be calculated from equation (31).

$$\frac{dC_w}{dk} = \frac{C_{w1} - C_{w2}}{K_1 - K_2} = \frac{0.001427}{0.03425} = 0.041652 \quad (31)$$

Where C_{w1} is the wave making resistance coefficient at Fn_h is 0.57 and blockage ratio $K_1 = 0.1073$ and C_{w2} is the wave making resistance coefficient at Fn_h is 0.57 and blockage ratio $K_2 = 0.0073$.

The form factor representing the three dimensionality of ship form an increasing viscous resistance was deduced based on measured resistance data in shallow water conditions for two blockage ratio. It was found that 3D effect is more significant (almost 50% higher) for higher ship/canal blockage ratio.

6.1. Discussion and future work

This research has provided and documented very useful data regarding container ships sailing in shallow water, restricted channel or very narrow canals. It also experimentally approach a very interesting phenomenon (squat, trim, and increased resistance) in shallow and narrow waters. Implementing uncertainty analysis on the test procedures and results increases the reliability and quality of the research findings. All plots are produced in nondimensional format such that they can be extended to similar cases. For example the increasing in total resistance coefficient in Case I when the model run for H/T = 1.78 which present model draft 0.18 is 14% compared with the same case for H/T = 2.5 at $Fn_h = 0.57$. The same for sinkage/l_{pp} is increasing with 37.7%. Furthermore, the model trim by bow increase with 3.1% when the H/T for model decrease from 2.5 to 1.78 at the same case and $Fn_h = 0.57$. Moreover, all data will be used as a benchmark to verify our planned CFD simulation analysis.

Finally the study revealed that ship motions behaviour significantly change in shallow water and restricted water compared to those in deep water. It would be very interesting to investigate experimentally high speed ship model more than $Fn_h = 0.6$ for Case II and Case III. Another piece of interesting future study would be to investigate the effect of trim on containership sailing characteristics in shallow waters and restricted water at critical and supercritical speed range using the KCS model.

Acknowledgements

The results were obtained conducted at the Kelvin Hydrodynamics Lab at the University of Strathclyde.

References

Alderf, N., Lefrançois, E., Sergent, P., Debaillon, P., 2011. Dynamic ship response integration for numerical prediction of squat in highly restricted waterways. Int. J. Numer. Methods Fluids 65 (7), 743–763.
Barrass, B., Derret, D.R., 2012. Ship Stability for Masters and Mates, seventh ed. Elsevier Ltd, USA.
Conn, J.F.C., Lackenby, H., Walker, W.P., 1953. BSRA Resistance experiments on the Lucy Ashton. Transactions of the Royal Institution of Naval Architects 95, 350–436.
Constantine, T., 1961. The behaviour of ships moving in restricted waterways. In: Proceedings of the Institution of Civil Engineers, E-ISSN 1753-7789, vol. 19. pp. 549–562 4, AUGUST 1961.
Delefortrie, G., Vantorre, M., Eloot, K., Vewilligen, J., Lataire, E., 2010. Squat prediction in muddy navigation areas. Ocean Eng. 37 (16), 1464–1476 November 2010.
Gourlay, T., 2008a. Sinkage and trim of a fast displacement catamaran in shallow water. J. Ship Res. 52 (3), 175–183.
Gourlay, T., 2008b. Slender-body methods for predicting ship squat. Ocean Eng. 35 (2), 191–200.
Gourlay, T., 2008c. Sinkage and trim of two ships passing each other on parallel courses. Ocean Eng. 36 (14), 1119–1127 October 2009.
GUM, I., 2008. Guide to the Expression of Uncertainty in Measurement, (1995), with Supplement 1, Evaluation of Measurement Data, Jcgm 101: 2008. Organization for Standardization, Geneva, Switzerland.
Havelock, T.H., 1908. The propagation of groups of waves in dispersive media, with application to waves on water produced by a travelling disturbance. Proc. R. Soc. Lond. - Ser. A Contain. Pap. a Math. Phys. Character 81 (549), 398–430. https://doi.org/10.1098/rspa.1908.0097.
ITTC, 2002. Testing and extrapolation methods resistance. In: ITTC Procedure 7.5-02 -02-01.
ITTC, 2011. Fresh water and seawater Properties. In: ITTC Procedure 7.5-02-01-03.
ITTC, 2014. Example for uncertainty analysis of resistance tests in towing tank. In: ITTC Procedure 7.5-02 -02-02.1.
ITTC, 2017. Uncertainty analysis instrument calibration. In: ITTC Procedure 7.5-01-03-01.
JI, s. h., Ouahsine, A., Smaoui, H., Sergent, P., 2012. 3-D Numerical simulation of convoy-Generated waves in a restricted waterway. J. Hydrodyn. Ser. B 24 (3), 420–429 1 July 2012.
Kazerooni, M.F., Seif, M.S., 2013. Experimental evaluation of ship squat in shallow waters. Waters. J Braz. Soc. Mech. Sci. Eng. 36, 559–569. https://doi.org/10.1007/s40430-013-0114-y. 2014.
Kazerooni, M.F., Seif, M.S., 2014. Experimental study of a tanker ship squat in shallow Jurnal Teknologi. Sci. Eng. 66 (2), 15–20 2014.
Larsson, L., Raven, H.C., Paulling, J.R., 2010. The Principles of Naval Architecture Series, Ship Resistance and Flow. The Society of Naval Architects and Marine Engineers, Jersey City, New Jersey.
Lataire, E., Vantorre, M., Deleortrie, G., 2012. A prediction method for squat in restricted and rectangular fairways. Ocean Eng. 55, 71–80 2012.
Millward, A., 1996. A review of the prediction of squat in shallow water. J. Navig. 49 (1), 77–88 January 1996.
Molland, Anthony, F., 2017. Ship Resistance and Propulsion: Practical Estimation of Ship Propulsive Power/Anthony F. Molland, Stephen R. Turnock, Dominic A. Hudson, second ed. .
Sergent, P., Lefrançois, E., Mohamad, N., 2014. Virtual bottom for ships sailing in restricted waterways (unsteady squat). Ocean Eng. 110, 205–214 Part A, 1 December 2015.
SIMMAN, 2008. Geometry and conditions. Retrieved from. http://www.simman2008.dk/KCS/kcs_geometry.htm, Accessed date: 15 March 2018.
Suez Canal Authority, 2018. Canal characteristics. Retrieved from. https://www.suezcanal.gov.eg/English/Pages/default.aspx, Accessed date: 30 March 2018.
Terziev, M., Tezdogan, T., Oguz, E., Gourlay, T., Demirel, Y.K., Incecik, A., 2018. Numerical investigation of the behaviour and performance of ship advancing through restricted shallow waters. J. Fluids Struct. 76, 185–215.
Tezdogan, T., Incecik, A., Turan, O., 2015. A numerical investigation of the squat and resistance of ships advancing through a canal using CFD. J. Mar. Sci. Technol. 21, 86–101. https://doi.org/10.1007/s0073-015-0334-1. 2016.
Toxopeus, S., 2011. Viscous-flow calculations for KVLCC2 in deep and shallow water. In: International Conference on Computational Methods in Marine Engineering Lisbon, Portugal.

Tuck, E.O., 1966. Shallow-water flows past slender bodies. J. Fluid Mech. 26 (1), 81–95 September 1966.
WORLD MARITIME NEWS, 2016. Grounding in Suez canal. Retrieved from. https://search.worldmaritimenews.com/search?s=grounding+in+suez+canal&submit=submit, Accessed date: 30 March 2018.
Yuan, Z., Zhang, X., Ji, C., Jia, L., Wang, H., Incecik, A., 2018. Side wall effects on ship model testing in a towing tank. Ocean Eng. 147, 447–457.